

The Active Site of Melanopsin: The Biological Clock Photoreceptor

Sivakumar Sekharan,* Jennifer N. Wei, and Victor S. Batista*

Department of Chemistry, Yale University, New Haven, Connecticut 06520-8107, United States

S Supporting Information

ABSTRACT: The nonvisual ocular photoreceptor melanopsin, found in the neurons of vertebrate inner retina, absorbs blue light and triggers the “biological clock” of mammals by activating the suprachiasmatic nuclei (a small region of the brain that regulates the circadian rhythms of neuronal and hormonal activities over 24 h cycles). The structure of melanopsin, however, has yet to be established. Here, we propose for the first time a structural model of the active site of mouse melanopsin. The homology model is based on the crystal structure of squid rhodopsin ($\lambda_{\text{max}} = 490 \text{ nm}$) and shows a maximal absorbance ($\lambda_{\text{max}} = 447 \text{ nm}$) consistent with the observed absorption of the photoreceptor. The 43 nm spectral shift is due to an increased bond-length alternation of the protonated Schiff base of 11-*cis*-retinal chromophore, induced by N87Q mutation and water-mediated H-bonding interactions with the Schiff base linkage. These findings, analogous to spectral changes observed in the G89Q bovine rhodopsin mutant, suggest that single site mutations can convert photopigments into visual light sensors or nonvisual sensory photoreceptors.

Understanding structure/function relationships responsible for the activation of photoreceptors is a fundamental challenge of much current research interest, since these G-protein-coupled receptors are involved in a variety of signal transmission pathways.¹ We focus on the transmembrane glycoprotein melanopsin found in the retinal ganglion cells of vertebrates, a photopigment that absorbs blue light and triggers activity of the suprachiasmatic nuclei—a small region of the brain that regulates the circadian rhythms of neuronal and hormonal activities over 24 h cycles.² We introduce a homology structural model of the active site of mouse melanopsin (Figure 1), based on the crystal structure of squid rhodopsin (hereafter called simply “melanopsin” and rhodopsin”),³ that provides insight into the molecular origin of spectral tuning, as determined by specific H-bonding interactions between the protonated Schiff base of 11-*cis*-retinal chromophore and water molecules bound at the active site.

In addition to rods and cones, the retina of vertebrates has intrinsically photosensitive retinal ganglion cells. These specialized neurons contain melanopsin, a photopigment involved in non-image-forming vision, including pupil responses to light and photoentrainment of the circadian rhythm.⁴ In primates and mice, melanopsin regulates visual processing, probably optimizing visual pathways according to the time of the day⁵ and spatial visual perception.⁶ Melanopsin resembles the photopigments of higher invertebrates (e.g., cephalopods and arthropods) in terms

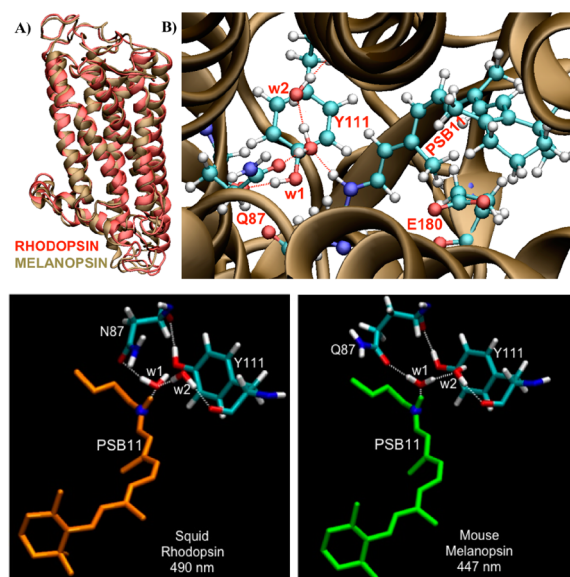


Figure 1. (A) Homology model of mouse melanopsin (brown) superimposed on the crystal structure of squid rhodopsin (red). (B) Active site of melanopsin. Bottom: H-bonding interactions with the protonated Schiff base responsible for spectral tuning in rhodopsin (left) and melanopsin (right).

of its primary sequence and photoactivation cascade. Contrary to the photobleaching pathway of vertebrate rhodopsin in rods and cones, melanopsin employs a bistable photon absorption mechanism⁷ that can recycle the photoproduct chromophore in the absence of the retinal pigment epithelium. Such a mechanism is typical of rhabdomeric photoreceptors (e.g., rhodopsin) and drives a phototransduction cascade mediated by Gq-type G protein but not transducin,⁸ similar to that of invertebrate Gq-coupled visual pigments.⁹ Thus, our homology model is based on the crystal structure of rhodopsin.³

Despite the significant differences in location, function, and size of vertebrate and invertebrate photoreceptors, they all have a retinyl chromophore covalently bound to an opsin apoprotein via protonated Schiff base linkage PSB11.¹⁰ One of their distinct characteristics is their maximal absorption wavelength (λ_{max}). For example, rhodopsins (RH1 rod pigments) absorb at $\sim 500 \text{ nm}$, whereas cone middle- and long-wavelength-sensitive (M/LWS) pigments absorb at $\sim 510\text{--}560 \text{ nm}$.¹¹ The λ_{max} of melanopsin remains unclear, probably due to difficulties in its expression and purification.^{9,12}

Received: September 4, 2012

Published: November 12, 2012

For example, the action spectrum (wavelength sensitivity) of human melanopsin (opn4 pigments) was determined to be ~446–477 nm.¹³ However, when the derived action spectrum was fitted by the absorption spectrum of vitamin A₁-based photopigment, human melanopsin λ_{max} was between 481 and 484 nm.¹⁴ A recent experimental study based on bovine rhodopsin ($\lambda_{\text{max}} = 499$ nm) as a reference point determined $\lambda_{\text{max}} = 467$ nm for melanopsin (i.e., a 32 nm blue-shift compared to rhodopsin).¹⁵ Clearly, a consensus on the wavelength of maximal absorbance has yet to be reached. It is important to develop structural models that address these issues and offer insights into the photochemical properties of melanopsin.

The molecular origin of spectral tuning in melanopsin remains elusive, partially due to the lack of structural models. In the past, amino acid (aa) substitutions were shown to induce interconversion within archaeal rhodopsins. For example, D85T and A215T mutants convert bacteriorhodopsin (light-driven proton pump) into halorhodopsin (chloride ion pump)¹⁶ and sensory rhodopsin (phototaxis receptor).¹⁷ We implement a similar approach to address the conversion of the active site of rhodopsin into the corresponding active site of melanopsin. The rationale behind interconversion is that the photochemical properties of melanopsin are very similar to those of invertebrate photopigments.¹⁵

QM/MM models were built by using the two-layer ONIOM scheme with electronic-embedding (EE),¹⁸ as implemented in Gaussian09.¹⁹ The QM layer included the retinyl chromophore PSB11 and the side-chain N–H moiety of K305, treated according to DFT at the B3LYP/6-31G(d) level. The MM layer included the rest of the protein, as described by the AMBER96 molecular mechanics force field.²⁰ The interface between QM and MM layers was treated by using the standard H-link atom scheme. According to the ONIOM QM/MM(EE) scheme, the QM/MM electrostatic interactions are included in the QM calculations, and therefore the QM wave function is polarized by the MM point charges.¹⁸ This procedure follows earlier studies,^{21–23} showing that the retinal-binding pocket of functionally related rhodopsins could be built by using QM/MM relaxation methods. In fact, the evolution of red and green vision in mammals,²¹ and blue and violet vision in butterflies,²² and the origin of the spectral shift between channelrhodopsin and bacteriorhodopsin²³ have been successfully studied by using QM/MM models of the retinal-binding pocket.

The first step involved the preparation of an optimized structure of rhodopsin, as previously reported according to the ONIOM QM/MM(EE) scheme.²⁴ Rhodopsin is composed of 448 aa residues, whereas melanopsin is made up of 521 residues. The amino acid sequences were aligned (see SI for details) and mutated according to the primary sequence of melanopsin. In total, 163 aa's were mutated, including 6 negatively charged (Q28D, F105E, K109E, N229E, A235E, K239E) and 12 positively charged (K61R, K63R, Q66R, K146R, H149K, M225R, S228R, K232R, E245R, K248R, G252R, R258K). Of the 38 aa's that are within 4.5 Å from an atom of the retinyl chromophore, 18 residues distributed across the seven transmembrane regions (Figure 2) have been mutated. To minimize the structural changes and to preserve the natural shape of the protein, the full structure was relaxed through a two-step procedure: the mutated residues were relaxed, keeping fixed the rest of the protein, and then the whole protein was relaxed without any constraints. Figure 1A shows an overlay of the resulting optimized QM/MM structural models of rhodopsin and melanopsin. The mutated residues in the active site

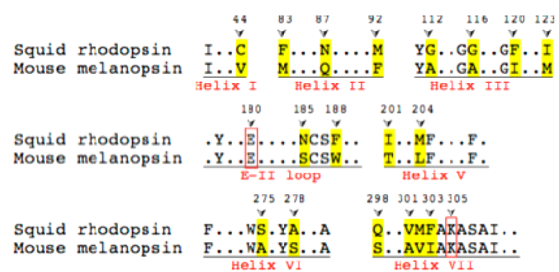


Figure 2. Sections of the primary sequences of rhodopsin and melanopsin including amino acid residues within 4.5 Å radius of any atom of the retinyl pSB chromophore, highlighted in yellow. Retinal-binding site K305 and counterion E180 (red boxes) are conserved in the two pigments. Residue numbers correspond to the primary sequence of rhodopsin.

correspond to C44V in helix I; F83M, N87Q, and M92F in helix II; G112A, G116A, F120I, and I123 M in helix III; N185S and F188W in the EII-loop; I201T and M204L in helix V; S274A and A278S in helix VI; and Q298S, V301A, M302V, and F303I in helix VII (using the amino acid numbering of rhodopsin, Figure 2). Both the retinal-binding site K305 and the negatively charged counterion E180 are conserved. The two internal water molecules (w1, w2) near the SB region in rhodopsin were also retained in the melanopsin model.

The chromophore geometries are significantly different along the polyene chain (Figure 3), because amino acid substitutions in helix III and helix VII involve removal of bulky side chain and/or aromatic rings, releasing the underlying stiffness of the pSB

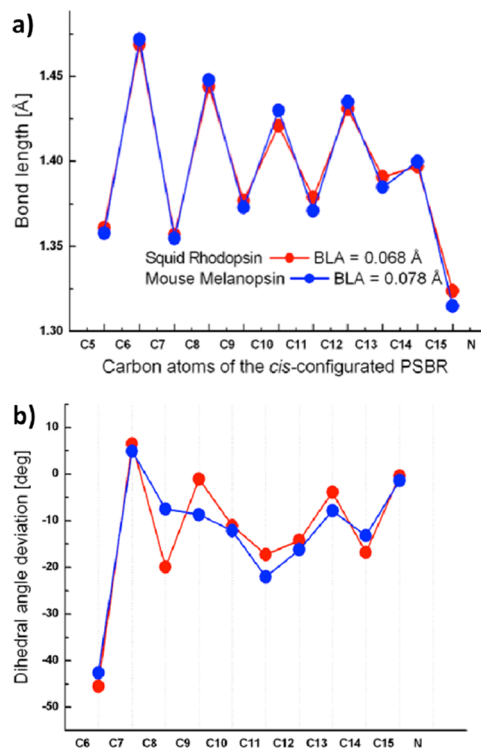


Figure 3. (a) Bond length and (b) dihedral angle deviation along the retinyl pSB polyene chain of rhodopsin (red) and melanopsin (blue). Dihedral angle deviations are from either *cis* (0°) or *trans* (180°) configurations. Average bond length alternation values, defined as the average of the bond lengths of single minus double bonds (C5 to SBN⁺ moiety), are also given. For details, see SI.

backbone. This induces more planar dihedral angles along C7–C8–C9–C10 in melanopsin compared to rhodopsin (Figure 3b). Consequently, the pocket becomes wider, and water molecules rearrange to stabilize H-bonding interactions. In the case of the F188W substitution, the aromatic ring originally positioned close to the C9-methyl group is displaced with a five-membered pyrrole ring facing away from the polyene chain. This structural rearrangement creates space and bestows sufficient flexibility for a more planar retinyl chromophore in melanopsin compared to rhodopsin. The distortion required to fit the retinyl pSB into the binding pocket is evenly distributed between the neighboring C11–C12 and C13–C14 double bonds (Figure 3b). As the single bonds become longer and double bonds become shorter (Figure 3a), the overall length of retinyl pSB conjugation (from C6 to SBN⁺ moiety) increases from 10.57 Å in rhodopsin to 10.70 Å in melanopsin. This property is reflected in the observed bond length alternation, defined as the average of single minus double bonds, which increases from 0.068 Å in rhodopsin to 0.078 Å in melanopsin. As previously observed,^{10,21,22,24} the increase/decrease in bond length alternation correlates with the decrease/increase in λ_{\max} of the pigments. In this case, due to the increase in bond length alternation, melanopsin exhibits a blue-shifted λ_{\max} compared to rhodopsin.

Internal water molecules are known to play a critical role in regulating H-bonding networks in rhodopsin. In the melanopsin active site, two bound water molecules (w1, w2) mediate five H-bonds next to the pSB linkage (Figure 1, bottom right); w1 bridges the pSB and Q87, and w2 H-bonds with w1 and the backbone carbonyl of Tyr111. In addition, the OH of Y111 is H-bonded to the backbone carbonyl of Q87, and the backbone NH of Q87 is H-bonded to the backbone carbonyl of M83. Compared to the active site of rhodopsin, the distance from the pSB linkage to Y111 and E180 decreases by 0.33 and 0.17 Å, and that to Q87 increases by 0.78 Å, due to rearrangements in the positions and orientations of w1 and w2 in melanopsin.

To validate the QM/MM models through direct comparisons with experiments, we computed the absorption and circular dichroism spectra of the chromophore, in the gas phase (QM) and in the protein (QM/MM) environment, using the *ab initio* multireference spectroscopy oriented configuration interaction method (SORCI+Q)²⁵ as implemented in the ORCA 2.6.19 program package.²⁶ The calculations were carried out using 6-31G(d) basis set on top of three-root (6e, 6o) CASSCF wave functions.²⁷ Note that the CAM-B3LYP functional has also been shown to yield bond length alternation values and excitation energies comparable to those obtained with the B3LYP functional.²⁸ The vertical excitation energies ($S_0 \rightarrow S_1$) as well as the oscillator and rotatory strengths were calculated for all structures discussed in this study (Table 1). The accuracy of the method is estimated to be ± 10 nm, and the present setup has been shown to yield results in good agreement with experimental measurements.^{21,22,24}

To determine the variance in λ_{\max} between rhodopsin and melanopsin, the difference in response of the excited and ground states to the external perturbation from the protein environment is calculated. The gas phase results in Table 1 correspond to PSB11 having the geometry of the chromophore in the QM/MM optimized protein of rhodopsin and melanopsin, absorbing 604 and 612 nm, respectively.²⁹ In both proteins, the counterion Glu180 balances the positive charge on the SB and is the single largest contributor to the opsin shift (blue-shift ~ 120 nm).^{10,21,22,24,30–32} The calculated absorption wavelengths of rhodopsin and melanopsin are 490 and 447 nm, in very good

Table 1. Calculated SORCI+Q First Vertical Excited-State ($S_0 \rightarrow S_1$) Absorption Wavelengths (λ), Oscillator (f) and Rotatory (R) Strengths, and Changes in the Ground- and Excited-State Dipole Moments ($\Delta\mu$) of PSB11 in Gas Phase (QM) and Protein (QM/MM) Environments of Photopigments

photopigment	gas phase		protein				expt λ (nm) ^a
	λ (nm)	f (au)	λ (nm)	f (au)	R (au)	$\Delta\mu$ (D)	
squid rhodopsin	604	0.9	490	1.1	0.3	11.7	488
mouse melanopsin							
with w1	612	1.0	447	1.2	0.4	10.9	446
without w1	635	1.0	484	1.2	0.2	11.1	484
bovine rhodopsin							
wild-type	616	1.2	495	1.4	0.2	12.1	499
G89Q mutant	614	1.2	481	1.4	0.1	11.9	–

^aValues are from refs 8a, 13, 14, and 15.

agreement with experimental values of 488 and 446 nm, respectively.^{13a,14} The blue-shift separating the two pigments can be traced back to the decrease in polarization of the retinyl chromophore in melanopsin. This property is evident in the calculated change in dipole moment ($\Delta\mu$) between the ground (S_0) and excited (S_1) states of the retinyl pSB, which decreases from 11.7 D in rhodopsin to 10.9 D in melanopsin. In addition, the calculated oscillator (f) and rotatory strengths (R) also increase from rhodopsin to melanopsin (f from 1.1 to 1.2 au, and R from 0.3 to 0.4 au).

Furthermore, the spectral shifts induced by individual amino acid residues are analyzed by zeroing the charges of the 18 non-conserved aa residues in the active site of melanopsin (Figure 4).

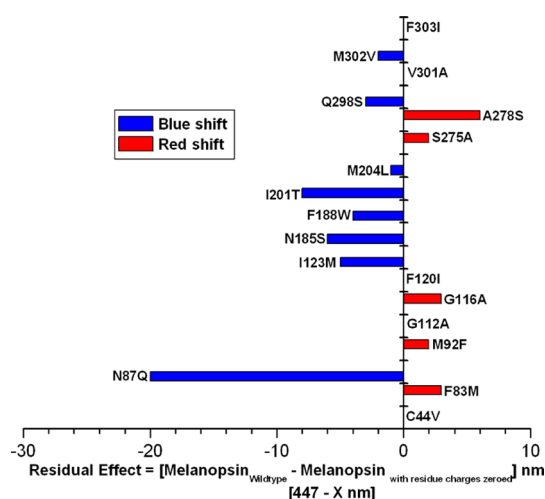


Figure 4. Electrostatic contribution of the 18 amino acid substitutions in the active site of melanopsin. Red/blue bars indicate red/blue-shifts arising due to zeroing of charges at that site.

The most significant shift arises from the N87Q (–20 nm) mutant. Four substitutions (C44V, G112A, V301A, F301I) do not contribute to the overall spectral shift, and the remaining 13 residues induce spectral shifts in the ± 10 nm range that are nonadditive. Therefore, we suggest that mutation of N87Q and the resulting increase in bond length alternation of the retinyl pSB are the two main factors responsible for the origin of the blue-shift of melanopsin when compared to rhodopsin. In addition, we have determined the influence of internal water

molecules by comparing the spectra of the models after reoptimizing the structures in the absence of w1 and w2. In the absence of w1 or w2, the total number of H-bonds is reduced from five to two, keeping only the H-bonds between the Q87 and Y111 and between w2 and Y111. While loss of w2 has no influence on the calculated λ_{max} , the absence of w1 decreases the bond length alternation of the retinyl pSB from 0.078 to 0.069 Å, increases the dipole moment from 10.9 to 11.1 D, and increases the calculated λ_{max} from 447 to 484 nm. Also, the small increase in the calculated dipole moment can be attributed to the reorientation of the SB due to decrease in the distance between the SBN and OH atom of Y111 (from 3.08 to 2.95 Å). Therefore, our analysis supports the presence of bound water molecules in the active site and participation of water-mediated H-bonding networks in spectral tuning. We predict that in the presence of w1, λ_{max} is as low as 447 nm, while in the absence of w1, λ_{max} is as high as 484 nm.

Interestingly, site N87 corresponds to site G89 in bovine rhodopsin. Natural mutations at site 89 are known to cause retinal degenerative diseases, such as autosomal dominant retinitis pigmentosa.³³ However, to our knowledge, the G89Q mutant has not been reported before. Therefore, to validate the results obtained from melanopsin, we introduced G89Q mutant in the QM/MM optimized structure of bovine rhodopsin. Similar to the effect of N87Q in melanopsin, G89Q induces a blue-shift of 14 nm and moves the λ_{max} from 495 to 481 nm. As site 89 is situated in the transmembrane helix II and positioned almost ~ 10 Å from the retinyl pSB, increasing the side chain (from G to Q) interferes with the conserved interhelical interactions, which may influence the wavelength sensitivity of rhodopsin. These results should stimulate experimental verification from site-directed mutagenesis analysis that might correlate our G89Q results with physiological data.

In conclusion, this theoretical study has characterized the structure and spectral tuning mechanism of mammalian melanopsin at the molecular level. Understanding the structure, wavelength sensitivity, and spectral tuning of melanopsin is the first step toward manipulating the regulation of circadian rhythms. As light is a powerful regulator of the circadian system, the findings not only allow us to optimize the use of light in therapeutic applications but also pave the way for converting a visual light sensor into a nonvisual sensory photoreceptor, although the physiological output of the photoreceptor depends on its cellular environment and signaling interactions.

■ ASSOCIATED CONTENT

📄 Supporting Information

Computational details and mutation data. This information is available free of charge via the Internet at <http://pubs.acs.org>. The PDB file (5SJV.pdb) of the homology model of mouse melanopsin will be provided upon request from the authors.

■ AUTHOR INFORMATION

Corresponding Author

sivakumar.sekharan@yale.edu; victor.batista@yale.edu

Notes

The authors declare no competing financial interest.

■ ACKNOWLEDGMENTS

We acknowledge supercomputer time from the National Energy Research Scientific Computing Center (NERSC) and support from the National Science Foundation (NSF CHE-0911520).

■ REFERENCES

- (1) Gether, U.; Kobilka, B. *J. Biol. Chem.* **1998**, *273*, 17979.
- (2) (a) Provencio, I.; Jiang, G.; DeGro, W. J.; Hayes, W. P.; Rollag, M. D. *Proc. Natl. Acad. Sci. U.S.A.* **1998**, *95*, 340. (b) Provencio, I.; Rodriguez, I. R.; Jian, G.; Hayes, W. P.; Rollag, M. D. *J. Neurosci.* **2000**, *20*, 600.
- (3) Murakami, M.; Kouyama, T. *Nature* **2008**, *453*, 363.
- (4) (a) Hattar, S.; et al. *Nature* **2003**, *424*, 76. (b) Lucas, R. J.; et al. *Science* **2003**, *299*, 245. (c) Panda, S.; et al. *Science* **2003**, *301*, 525.
- (5) Barnard, A. R.; Hattar, S.; Hankins, M. W.; Lucas, R. J. *Curr. Biol.* **2006**, *16*, 389.
- (6) Ecker, J. L.; et al. *Neuron* **2010**, *67*, 49.
- (7) Koyanagi, M.; Terakita, A. *Photochem. Photobiol.* **2008**, *84*, 1024.
- (8) (a) Shichida, S.; Tokunaga, F.; Yoshizawa, T. *Biochim. Biophys. Acta: Bioenerg.* **1978**, *504*, 413. (b) Terakita, A.; Hariyama, T.; Tsukahara, Y.; Katsukar, Y.; Tashiro, H. *FEBS Lett.* **1993**, *330*, 197. (c) Terakita, A.; Yamashita, T.; Tachibana, S.; Shichida, Y. *FEBS Lett.* **1998**, *439*, 110. (d) Yarfitz, S.; Hurley, J. B. *J. Biol. Chem.* **1994**, *269*, 14329.
- (9) Terakita, A.; Tsukamoto, H.; Koyanagi, M.; Sugahara, M.; Yamashita, T.; Shichida, Y. *J. Neurochem.* **2008**, *105*, 883.
- (10) Sekharan, S.; Morokuma, K. *J. Am. Chem. Soc.* **2011**, *133*, 19052.
- (11) Yokoyama, S. *Annu. Rev. Genomics Hum. Genet.* **2008**, *9*, 259.
- (12) (a) Newman, L. A.; Walker, M. T.; Brown, L.; Cronin, T. W.; Robinson, P. R. *Biochemistry* **2003**, *42*, 12734. (b) Koyanagi, M.; Kubokawa, K.; Tsukamoto, H.; Shichida, Y.; Terakita, A. *Curr. Biol.* **2005**, *15*, 1065.
- (13) (a) Brainard, G. C.; et al. *J. Neurosci.* **2001**, *21*, 6405. (b) Hankins, M. W.; Peiron, S. N.; Foster, R. G. *Trends Neurosci.* **2008**, *31*, 27.
- (14) (a) Berson, D. M.; Dunn, F. A.; Takao, M. *Science* **2002**, *295*, 1070. (b) Walker, M. T.; Brown, R. L.; Cronin, T. W.; Robinson, P. R. *Proc. Natl. Acad. Sci. U.S.A.* **2008**, *26*, 8861. (c) Mure, L. S.; et al. *PLoS* **2009**, *4*, e5991.
- (15) Matsuyama, T.; Yamashita, T.; Imamoto, Y.; Shichida, Y. *Biochemistry* **2012**, *51*, 5454.
- (16) Sasaki, J.; Brown, L. S.; Chon, Y. S.; Kandori, H.; Maeda, A.; Needleman, R.; Lanyi, J. K. *Science* **1995**, *269*, 73.
- (17) Spudich, E. N.; et al. *J. Mol. Biol.* **2012**, *415*, 455.
- (18) Vreven, T.; Morokuma, K.; Farkas, O.; Schlegel, H. B.; Frisch, M. *J. Comput. Chem.* **2003**, *24*, 760.
- (19) Frisch, M. J.; et al. *Gaussian 09*, revision A.02; Gaussian, Inc.: Wallingford, CT, 2009.
- (20) Cornell, W. D.; et al. *J. Am. Chem. Soc.* **1995**, *117*, 5179.
- (21) Sekharan, S.; Katayama, K.; Kandori, H.; Morokuma, K. *J. Am. Chem. Soc.* **2012**, *134*, 10706.
- (22) Sekharan, S.; Yokoyama, S.; Morokuma, K. *J. Phys. Chem. B* **2011**, *115*, 15380.
- (23) Welke, K.; Frähmcke, Watanabe, H. C.; Hegemann, P.; Elstner, M. *J. Phys. Chem. B* **2011**, *115*, 15119.
- (24) Sekharan, S.; Altun, A.; Morokuma, K. *Chem. Eur. J.* **2010**, *16*, 1744.
- (25) Neese, F. A. *J. Chem. Phys.* **2003**, *119*, 9428.
- (26) Neese, F. *ORCA*, v.2.6; Universität Bonn: Bonn, Germany, 2007.
- (27) Roos, B. O.; Taylor, P. R. *Chem. Phys.* **1998**, *48*, 157.
- (28) Zhao, Y.; Truhlar, D. G. *J. Phys. Chem. A* **2006**, *110*, 10478.
- (29) Sekharan, S.; Weingart, O.; Buss, V. *Biophys. J.* **2006**, *91*, L07.
- (30) Sekharan, S.; Altun, A.; Morokuma, K. *J. Am. Chem. Soc.* **2010**, *132*, 15856.
- (31) (a) Mathies, R.; Stryer, L. *Proc. Natl. Acad. Sci. U.S.A.* **1976**, *73*, 2169. (b) Sakmar, T. P.; Franke, R. R.; Khorana, H. G. *Proc. Natl. Acad. Sci. U.S.A.* **1989**, *86*, 8309.
- (32) (a) Gascon, J. A.; Sproviero, E. M.; Batista, V. S. *Acc. Chem. Res.* **2006**, *39*, 184. (b) Sekharan, S.; Sugihara, M.; Buss, V. *Angew. Chem., Int. Ed.* **2007**, *46*, 269. (c) Altun, A.; Yokoyama, S.; Morokuma, K. *J. Phys. Chem. B* **2008**, *112*, 6814.
- (33) Bosch, L.; Ramon, E.; del Valle, L. J.; Garriga, P. *J. Biol. Chem.* **2003**, *278*, 20203.